Management Analytics and Social Insights

www.masi.reapress.com

Manag. Anal. Soc. Insights. Vol. 1, No. 2 (2024) 154–170.

Paper Type: Original Article

Managing 3D Printing Processes: Enhancing Pick-and-Place Machine Quality with Taguchi and Principal Component Analysis

Chien-Yi Huang[1,*], Ya-Wei Chung[1]

[1] Department of Industrial Engineering and Management, National Taipei University of Technology, Taipei, Taiwan; Jayhuang@ntut.edu.tw; Chungyw20152@gmail.com.

Citation:

Received: 12 May 2024 *Revised: 16 June 2024* *Accepted: 15 July 2024*	Yi Huang, CH., & Chung, Ya-Wei. (2024). Managing 3D printing processes: enhancing pick-and-place machine quality with taguchi and principal component analysis. *Management analytics and social insights, 1*(2), 154-170.

Abstract

3D printing techniques are now thriving and extensively used in producing cultural and creative individualized goods. In the present economic development of Taiwan, the electronics manufacturing industry has the highest output value. This study aimed to introduce 3D printing techniques in the electronics manufacturing sector, taking the printing of automatic insertion parts clip bodies as an example. The assembling will fail if an object's quality characteristics fail to meet the standard. This study established four key quality characteristics: the inside diameter of the left and right holes, the outside diameter of the locating point, the height of the locating point, and the middle recess thickness. The tolerance determination of the Taguchi quality loss method was used to establish the manufacturer tolerance of the print object. A printing parameter optimization experiment was then conducted to upgrade the overall quality. Principal Component Analysis (PCA) was used to propose the optimum parameter combination: PLA material, a fill thickness of 0.16mm, a wall thickness of 0.8mm, a bottom/top thickness of 1.2mm, an infill density of 50%, a printing speed of 20mm/s, and an extruder head temperature of 220℃. Finally, the benefit was assessed, considering the required cost for production, including the purchase cost, depreciation, amortized cost, creation of the 3D model file, the labour cost of operating the printer object subsequent surface treatment and component assembly, and the material cost for the print object and support structure.

Keywords: 3D printing, Automatic insertion, Manufacturer tolerance, Taguchi method, Benefit assessment.

1 | Introduction

In recent years, the application of 3D printing techniques has developed rapidly. It has been applied to consumables, automobiles, medical biotechnology, education, aerospace, industrial machinery, and food industries. Suppliers are actively pushing 3D metal printing for automobile precision parts and components, and this area is expected to be competitive in the 3D printing industry. However, key factors such as equipment, materials, service, software, and patents face challenges. As 3D printing techniques become popular, the mould unloading cost and time can be significantly reduced during the prototype production stage, and the product test time and time-to-market can be shortened. Therefore, in shortening product life

Corresponding Author: Jayhuang@ntut.edu.tw

https://doi.org/10.22105/w35wyr75

cycles and market demand for small-volume production of various items, 3D printing techniques are a key industrial transformation and upgrading technology.

The industrial output of 3D printing applications accounts for 48.86% of the present economic development structure. The electronics manufacturing industry has the highest GDP value among various industries. Investments in the manufacturing industry reserve the manufacturing industry by creating employment, of which 3D printing forms a stream. The German Fraunhofer Laser Technology Institute promotes rudimental metal 3D printing by providing small and medium-sized enterprises with comprehensive support and training for various stages of 3D printing.

3D printing is a rapid-forming technique in which the 3D structural model of a product is built using computer-aided design software or a 3D scanner. The file is saved in the STL or OBJ format, and the 3D plot file is cut layer by layer with slicing software. The STL file is converted into the G-code file format, which can read print command parameters and then loaded into the machine for printing, as shown in *Fig. 1*. In the process of 3D printing, the product structure model file is taken as the original version, and material such as plastic filar, powdered metal, ceramic, or sand is stacked layer by layer according to the slice patterns to form an object to print out the product.

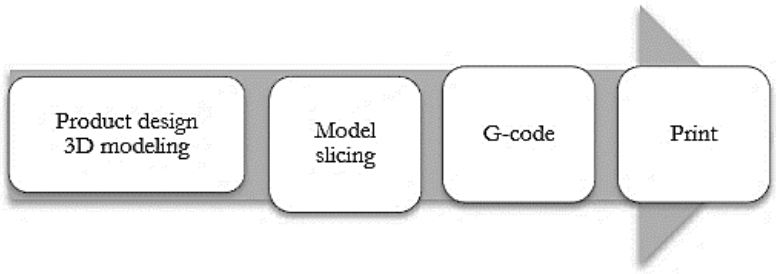

Fig. 1. 3D printing process.

1.1 | Research Motives

At present, 3D printing techniques are thriving. They have been extensively used to produce cultural and creative individualized goods, according to Bogue [1], and products with complex shapes that traditional production technologies cannot achieve. However, the study is still restricted to small quantities of customized products. 3D printing parameters include the printing material, fill thickness, wall thickness, temperature, and speed. Chen et al. [2] discussed the effect of material infill density, fill thickness, extruder head temperature, and printing speed parameters on the tensile strength of a product. Sanatgar et al. [3] printed PolyAmide (PA) fibre (nylon) and PolyLactic Acid (PLA) materials on a PA fabric surface. They indicated the impact of platform temperature, extruder head temperature, and printing speed on the adhesion force. However, the studies above only considered single-quality characteristics and did not consider all of the parameters of 3D printing that may limit the print quality and stability.

Related documents have discussed the correlation among specification stipulations, cost, and pricing practices in automobile, computer, and medical biotechnology product development and manufacturing processes [4–6]. There are no current product specifications for 3D printing manufacturing technology or standard specifications for judging product quality or identifying products that cannot meet requirements in the operational phase. In addition, previous research mostly discussed the application of 3D printing to the cultural and creative, medical treatment, and food areas. However, although the electronics manufacturing industry has the highest output value in the present economic development structure, few scholars have used 3D printing in the electronics manufacturing industry.

1.2 | Research Purpose

This study aimed to extend the 3D printing application area into the electronics manufacturing industry, taking production equipment components as examples to expand the application benefit of 3D printing techniques. The purposes are described below:

I. The tolerance determination of the Taguchi quality loss method was used to create the product specifications of 3D printing manufacturing technology for components of the electronics manufacturing industry so that products could meet requirements in the operational phase.

II. The effect of material selection and printing parameters on product quality characteristics was discussed using a Taguchi parameter design experiment, and the Principal Components Analysis (PCA) method was developed to measure multiple quality characteristic indicators. An optimum parameter level combination was proposed to confirm that the products would meet the specification above requirement.

III. Finally, the printing cost was discussed, and the benefit of using 3D printing techniques to produce the component was evaluated.

1.3 | Research Purpose

This study used a 3D printing technique to produce tools used for electronics manufacturing. First, the uses and characteristics of the components in the case were analyzed to sort out the overall external structure and assembly and determine the essential quality characteristics of the printed end product. Secondly, the tolerance determination of the Taguchi quality loss method was used to calculate the production specifications of various quality characteristics. The Taguchi experimental design was used to optimize the printing material and printing parameters. Multiple quality characteristics were considered in this study. Therefore, the PCA method was combined with various measurement indexes to propose the optimum printing parameter combination. Afterwards, the confirmation experiment was conducted, i.e., the optimum parameter combination was used for printing to judge whether the printing result was in the Confidence Interval (CI), determine the additivity of various factorial effects, and whether the print quality conformed with the tolerance specifications. Without error, the printed parts would be assembled and mounted on the machine for testing, ensuring stable operation. Finally, the benefit was assessed.

2 | Case Product Analysis

Electronic modules are combined with the PCB in the printed circuit board (PCB) assembly process to form the expected electronic loop. The electronic modules are classified into Surface Mount Components (SMC) and Through-Hole Mount Components (THMC) [7]. The THMC, including the resistor, capacitor, inductor, and diode elements, has a low manufacturing cost with a firm solder joint on the PCB, and it is universally used in electronic products with low functional density and high reliability. In the past, the THMC was inserted into the PCB manually. Still, in recent years, it has been implemented mainly through automatic insertion AI machines, increasing production efficiency and pick-and-place precision. AI machines are divided into vertical and horizontal types. The former is used for bulk elements, such as LED lighting and control systems. The latter is used for car audio devices and chargers. For vertical machines, the parts clip grips the electronic module from the feeder and sends it to the right position on the PCB for insertion, as shown in *Fig. 2*. The parts clip structure comprises a spring, a movable plate, and a clip body, as shown in *Fig. 3* and *Fig. 4*.

In this study, the 3D model of the clip body was built using Fusion360 drawing software, and the 3D model was sliced using Cura software. The principal component of the parts clip was printed with a Kraftmaker KM-V2 3D printer, a double extruder head printer of the Fused Deposition Modelling (FDM) process type. As the component was free of overhead geometric features, print support was not needed, and only one extruder head was used for operation, with a nozzle diameter of 0.4mm.

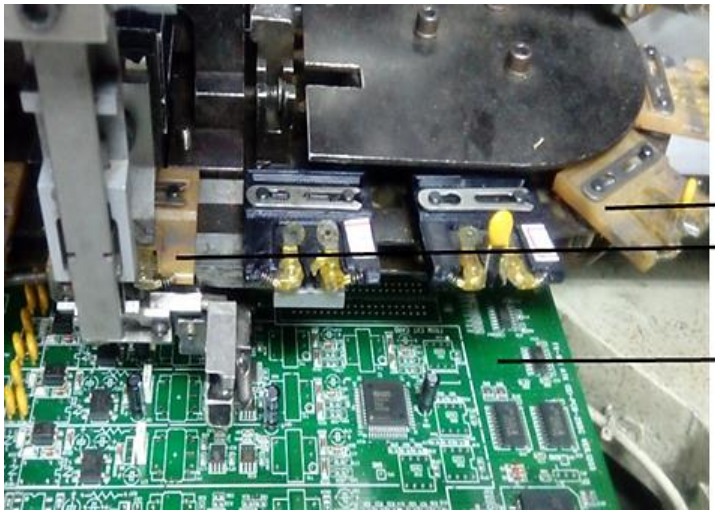

Fig. 2. Parts clip on AI machine.

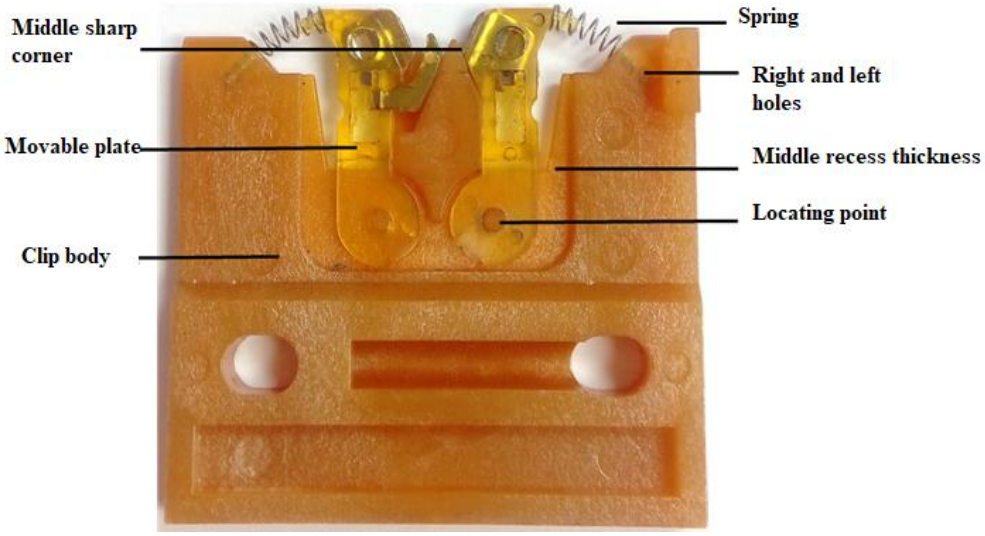

Fig. 3. Appearance of parts clip.

a. **b.** **c.**

Fig. 4. Parts clip structure: a. spring; b. movable plate; c. clip body.

2.1 | Discussion About Quality Characteristics

The clip body of the parts shall be assembled with a spring and movable plate after printing. Four key quality characteristics were established, as described below.

I. Inside diameter of the left and right holes (*Fig. 5. a*): the left and right holes of the clip body hold the spring, and the elastic force causes the clip body to clamp onto the capacitor pins. The spring cannot be inserted into the hole if the inside diameter is too small, and the spring will be loosened if the inside diameter is too large.

II. Outside diameter of the locating point (*Fig. 5. b*): the front and back sides of the clip body have two locating points placed in the movable plate's circular holes fixed to the clip body. Meanwhile, the movable plate can move side to side so that the capacitor pin can enter the sharp middle corner of the body and be clamped. The movable plate cannot be mounted if the outside diameter of the locating point is too large, and the movable plate will be loosened if the outside diameter of the locating point is too small.

III. Height of locating point (*Fig. 5.c*): the movable plate cannot be fastened if it is too low; if it is too high and exceeds the body plane, there will be interference with other components, and the inserter will fail.

IV. Middle recess thickness (*Fig. 5.d*): the middle recess of the clip body holds the movable plate, which is fixed by the locating above point. The movable plate cannot be mounted if the middle recess is too thick, and the movable plate will be loosened if the middle recess is too thin.

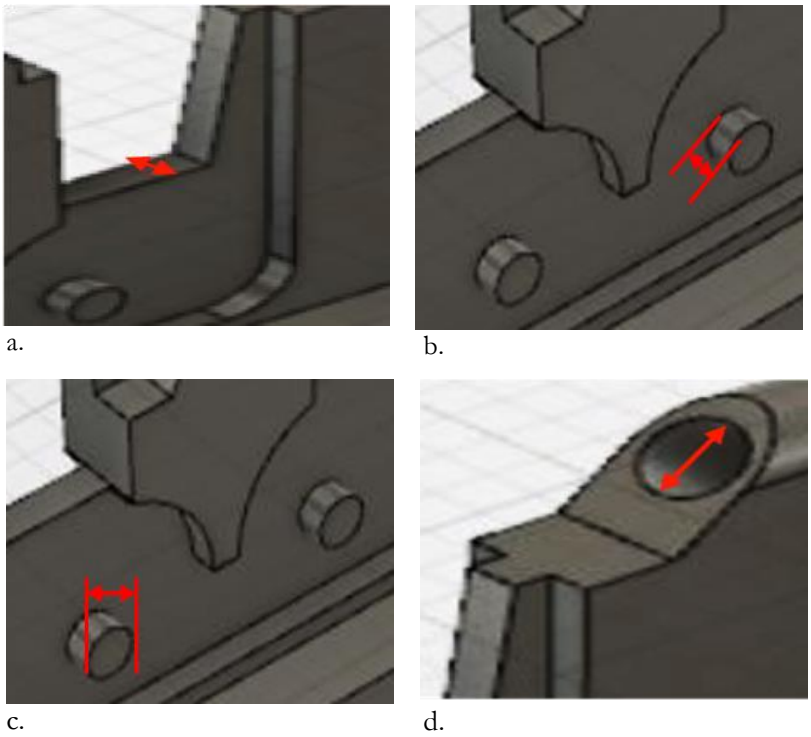

Fig. 5. Key quality characteristics of the parts clip body: a. inside diameter of hole; b. outside diameter of locating point; c. height of locating point; d. intermediate thickness.

3 | Calculating Specification Tolerance

The assembly may fail if the component quality characteristic fails to meet the standard. The Taguchi quality loss method [8, 9] considered the loss resulting from failed assembly and the rework cost from failing to meet specifications. The specifications and tolerance of the 3D printed components were established for the four quality above characteristics, expressed as *Eq. (1)*, in which the manufacturer tolerance Δ_{spec} is the manufacturer tolerance of the 3D printed component; A_{rework} is the loss resulting from the quality characteristic of the printed component failing to meet the specification tolerance (i.e. rework cost); A_{loss} is

the loss resulting from the component failing to work normally on the machine (or failing to be assembled smoothly) although the quality characteristic of the printed component meets the specification tolerance; and $\Delta_{tolerance}$ is the range of allowable error for the normal operation (or normal assembly) of the printed component on the machine.

$$\Delta_{spec}=\sqrt{\frac{A_{rework}}{A_{loss}}}\Delta_{tolerance}. \quad (1)$$

The printing machine cost, operator cost, and material cost of reprinting the component when the specification tolerance is exceeded must be considered in calculating the rework cost A_{rework} of the printed component, expressed as *Eq. (2)*, in which C_{3D} is the acquisition cost of the 3D printing machine, r_d is the depreciation rate per unit of time of the 3D printing machine, t_p is the time needed to print the component, r_o is the salary per unit time of the printing machine operator, and C_m is the printing material cost.

$$A_{rewoek} = (C_{3D} \times r_d \times t_p) + (t_p \times r_o) + C_m. \quad (2)$$

When calculating the loss A_{loss} resulting from the printed component not working normally although meeting the specification tolerance, the capacity loss and cost resulting from machine stoppage or maintenance when there is loosening of the component or machine interference in AI machine operations must be considered, including the cost A_{rework} for reprinting the component, expressed as *Eq. (3)*, in which t_s is the stop time, and r_p is the profit from the productive capacity per unit time of the AI machine.

$$A_{loss} = (t_s \times r_p) + A_{rework}. \quad (3)$$

The range of allowable error $\Delta_{tolerance}$ for normal operation of the component on the machine was calculated, as described below. For the four quality characteristics mentioned above, test samples of different-size features were designed and printed in turn and then assembled and mounted on the AI machine, respectively, to judge the allowable error range for smooth assembly or normal operation.

This case aimed at 3D printing of the component clip body of an AI machine, and related data were collected and calculated as follows. The acquisition cost of 3D printing machine C_{3D} was NTD 310,000, the depreciation rate per unit time of printing machine r_d was 0.02% (the depreciation cost per unit time of the printing machine was NTD 62), the time needed to print clip body t_p was one hour, the salary per unit time of printing machine operator r_o was NTD 168, the printing material cost C_m was NTD10, the stop time t_s, including problems related to finding and parts changing was 15 minutes. The profit from the productive capacity per unit time of AI machine r_p was NTD1,000/hr. The rework cost A_{rework} was NTD 240, and the loss from abnormal operation of clip body A_{loss} was NTD 490. The test results indicated that the range of allowable error $\Delta_{tolerance}$ for normal operation of the clip body on the machine was shown in *Table 1*. Finally, the specification tolerance Δ_{spec} of the four quality characteristics were calculated respectively (*Table 1*).

Table 1. Customer tolerance and manufacturer tolerance of various quality characteristics (mm).

Quality characteristics	Range of allowable error	Customer tolerance $\Delta_{tolerance}$	Manufacturer tolerance Δ_{spec}
The inside diameter of the left and right holes	2.30~2.40	0.050	0.035
The outside diameter of the locating point	1.46~1.64	0.090	0.063
Height of the locating point	0.65~0.98	0.168	0.118
Middle recess thickness	1.03~1.42	0.195	0.136

4 | Printing Parameter Optimization

This study experimentally designed the printing parameters of a 3D printing technique for the parts clip of an AI machine [10–12], hoping to determine the optimum printing parameter combination to upgrade the overall quality. The design of experiments and analysis results are described below.

4.1 | Pre-Experiment

To begin with, this study evaluated two printing bottom contact surfaces, the parts clip body backside down and body side down, to contact the printing platform, as shown in *Fig. 6. a* and *Fig. 6. b* In addition, if the printed object feature had a hanging design, the support structure would be built with the slicing software to stabilize the object during printing to prevent it from sagging or dropping. There were two scenarios: one with support and one without support. Afterwards, when printing the object's bottom layer, a peripheral frame was built to enhance the bottom strength and the bendability between the print object and the printing platform. There were two scenarios with and without a frame. The factor combinations considered in the pre-experiment are shown in *Table 2*.

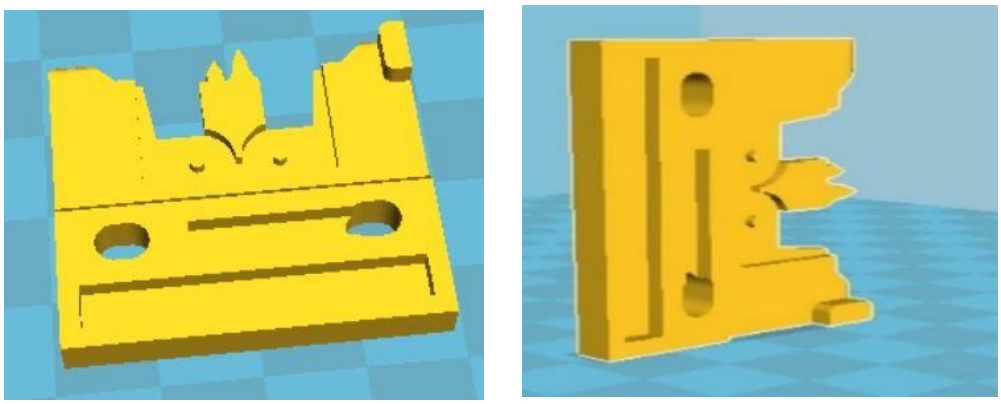

a. **b.**

Fig. 6. Printing bottom contact surface of the parts clip body: a. back side down; b. side down.

Table 2. Factor combinations of the pre-experiment.

Factor/level	Combination 1	
Bottom contact surface	Back side down	Side down
Support structure	No	Yes
Peripheral frame	No	Yes

The results indicated that if the parts clip body were printed using combination 2, the print object body would be damaged when removing the support material and the peripheral frame. In addition, during side-down printing, if the body locating point was too low, there would be a dimensional error, and the walls of the left and right holes would be incomplete, as shown in *Fig. 7*. Therefore, the subsequent printing experiment used the conditions of combination 1, i.e., a bottom contact surface with a back side down, no support structure, and no peripheral frame.

Fig. 7. Parts clip body printed using combination 2.

4.2|Control Factors and Levels

This experiment discussed the material characteristics and printing parameters that could influence the quality described above characteristics. The experimental control factors and levels are shown in *Table 3*, as described below:

I. Material: FDM process type 3D printing usually uses polylactide PLA material and Acrylonitrile Butadiene Styrene (ABS) resin. ABS resin material is stronger than PLA material but releases toxic gases during heating. High-Impact PolyStyrene (HIPS) and ABS resin materials have similar mechanical strengths. Therefore, this study evaluated PLA and HIPS materials.

II. Fill thickness: fill thickness refers to the thickness of each material layer used when printing the object. The smaller the fill thickness is, the finer the printed object surface will be; however, the process takes time. This study considered fill thicknesses of 0.16mm and 0.3mm.

III. Wall thickness: wall thickness refers to the thickness of the outer shell material while printing the object. It is generally set as a multiple of the nozzle bore. A thicker object wall contributes to enhancing the object surface's firmness. The nozzle bore was 0.4mm in this study, and the printed wall thicknesses were 0.8mm and 1.2mm.

IV. Bottom/top thickness: bottom/top thickness refers to the thickness of the topmost and bottommost stacked material. It is generally set as a multiple of the fill thickness. This study considered bottom/top thicknesses of 0.4mm and 1.2mm.

V. Infill density refers to the solid ratio of the material filling the print object. High infill density enhances the object's internal strength, but the process takes time and consumes material. An infill density higher than 20% approximates the entity. This study considered infill densities of 20% and 50%.

VI. Printing speed: slow printing may enhance the object's surface fineness, but the process takes time. This study considered printing speeds of 20 mm/s and 30 mm/s.

VII. Extruder head temperature: the extruder head temperature must be appropriate for the melting point of the printing material. If the temperature is too low, the material cannot adhere to the printing platform smoothly. The material's shaping quality will be affected if the temperature is too high. The material manufacturer suggested that the appropriate extruder head temperature ranges for HIPS and PLA material are 190~230℃ and 195~250℃, respectively. This study considered extruder head temperatures of 195℃ and 220℃.

4.3 | Experimental Configuration of Orthogonal Array

This study built an L8 orthogonal array for the experiment. The experimental configuration is shown in *Table 3*, including the seven control above factors with two levels. Each combination was printed twice, and two observations were made. The experimental order was random.

4.4 | Factorial Effect Analysis

The experimental results are shown in *Table 3*. As the four quality characteristics were the nominal-the-best characteristic of Taguchi quality, the Signal-to-Noise ratio (SN) of various parameter combinations could be calculated by *Eq. (4)*, in which $\bar{y}$ is the average of the observations, and s is the standard deviation of the observations. The response table and factor effect diagram of various quality characteristics is shown in *Table 4* and *Fig. 8*, respectively, to show the influence of multiple factors on the quality characteristic (SN).

$$\eta_{NTB} = 10 \times \log_{10}\left(\frac{\bar{y}^2}{s^2}\right). \quad (4)$$

Table 3. Experimental configuration and results of the L8 orthogonal array.

Experimental group	A	B	C	D	E	F	G	Observations			
	Material	Fill thickness	Wall thickness	Bottom/top thickness	Infill density	Printing speed	Extruder head temperature	Response value	1	2	SN
1	PLA	0.3	1.2	1.2	50	30	195	The inside diameter of the left and right holes	2.33	2.35	44.37
								Outside diameter of locating point	1.63	1.58	33.14
								Height of locating point	0.85	0.88	32.21
								Middle recess thickness	1.28	1.15	22.42
2	PLA	0.3	1.2	0.4	20	20	220	The inside diameter of the left and right holes	2.43	2.37	35.05
								Outside diameter of locating point	1.48	1.45	36.78
								Height of locating point	0.8	0.88	23.43
								Middle recess thickness	1.14	1.17	34.72
3	PLA	0.16	0.8	1.2	50	20	220	The inside diameter of the left and right holes	2.35	2.37	44.45
								Outside diameter of locating point	1.64	1.63	47.28
								Height of locating point	1.04	1	31.14
								Middle recess thickness	1.02	1.06	31.31
4	PLA	0.16	0.8	0.4	20	30	195	The inside diameter of the left and right holes	2.3	2.39	31.33
								Outside diameter of locating point	1.65	1.63	41.29
								Height of locating point	0.93	0.99	27.09
								Middle recess thickness	1.1	1.05	29.66
5	HIPS	0.3	0.8	1.2	20	30	220	The inside diameter of the left and right holes	2.27	2.14	27.6
								Outside diameter of locating point	1.57	1.43	23.61
								Height of locating point	0.72	0.74	34.26
								Middle recess thickness	1.17	1.19	38.43

Table 3. Continued.

Experimental group	A	B	C	D	E	F	G	Observations			
	Material	Fill thickness	Wall thickness	Bottom/top thickness	Infill density	Printing speed	Extruder head temperature	Response value	1	2	SN
6	HIPS	0.3	0.8	0.4	50	20	195	The inside diameter of the left and right holes	2.3	2.37	33.47
								Outside diameter of locating point	1.56	1.44	24.95
								Height of locating point	0.71	0.65	24.1
								Middle recess thickness	1.22	1.33	24.29
7	HIPS	0.16	1.2	1.2	20	20	195	The inside diameter of the left and right holes	2.11	2.05	33.81
								Outside diameter of locating point	1.6	1.58	41.02
								Height of locating point	0.77	0.78	40.8
								Middle recess thickness	1.23	1.01	17.15
8	HIPS	0.16	1.2	0.4	50	30	220	The inside diameter of the left and right holes	2.21	2.14	32.86
								Outside diameter of locating point	1.62	1.55	30.11
								Height of locating point	0.76	0.82	25.4
								Middle recess thickness	1.29	1.2	25.83

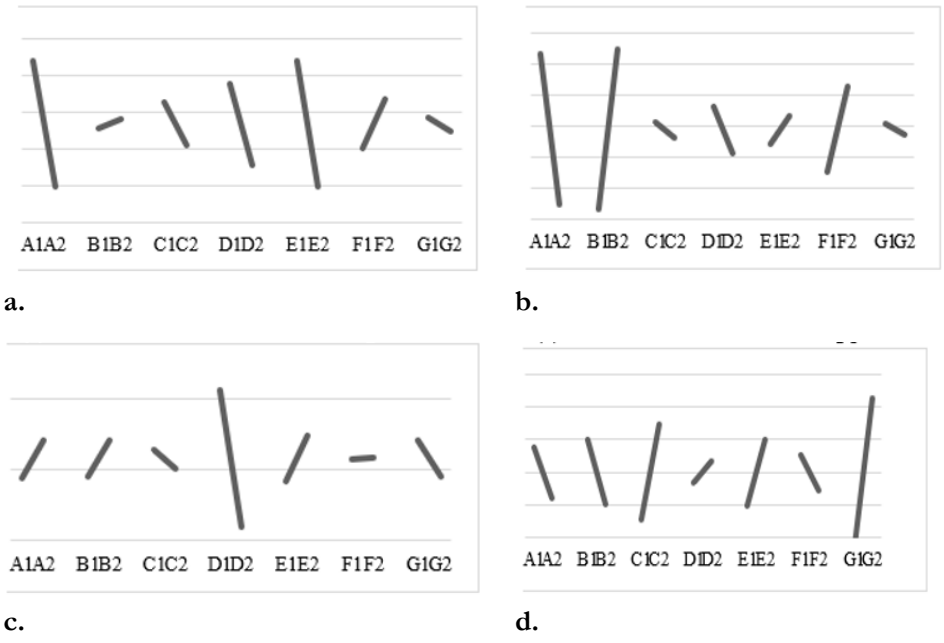

Fig. 8. Factor effect diagram of the printing parameter design; a. inside diameter of the left and right holes; b. outside diameter of the locating point; c. height of the locating point; d. middle recess thickness.

Table 4. Response table of the printing parameter design.

Control factor		A	B	C	D	E	F	G
The inside diameter of the left and right holes	Level 1	38.8	35.13	36.52	37.56	38.79	34.04	35.75
	Level 2	31.94	35.61	34.21	33.18	31.95	36.67	34.99
	Ideal level	A1	B2	C1	D1	E1	F2	G1
Outside diameter of locating point	Level 1	39.62	29.62	35.26	36.26	33.87	32.04	35.1
	Level 2	29.92	39.92	34.28	33.28	35.68	37.51	34.45
		A1	B2	C1	D1	E2	F2	G1
Height of locating point	Level 1	28.47	28.5	30.46	34.6	28.21	29.74	31.05
	Level 2	31.14	31.11	29.15	25.01	31.4	29.87	28.56
		A2	B2	C1	D1	E2	F2	G1
Middle recess thickness	Level 1	29.53	29.97	25.03	27.33	25.96	29.09	23.38
	Level 2	26.42	25.99	30.92	28.63	29.99	26.87	32.57
		A1	B1	C2	D2	E2	F1	G2

4.5 | Principal Component Analysis

As the ideal parameter combinations of the four quality characteristics were inconsistent, the mutually independent linear combinations were transformed for the probability correlated quality characteristics using Principal Component Analysis (PCA) to determine the optimum parameter combination [13, 14]. This approach aligns with established methodologies where PCA simplifies the complexity in multivariate data by reducing its dimensions, thus facilitating a more straightforward identification of the optimal settings [15]. PCA's effectiveness in optimizing process parameters is further supported by its ability to handle data intercorrelations that may affect the output quality [16], thus increasing interpretability and preserving the essential characteristics of the dataset [17]. The technique has been detailed in various studies, showcasing its utility in enhancing data analysis outcomes across different research fields [18]. It is renowned for its capacity to analyze data tables where observations are described by several inter-correlated quantitative variables [17]. Furthermore, PCA is instrumental in reducing the number of space dimensions while retaining the variance present in the dataset, which is crucial for efficient data analysis [19]. The analysis steps are described below.

Step 1: the original SN ratio matrix is standardized

M quality characteristics evaluate l parameter combinations. The original matrix D is built, where SN_1, SN_2, SN_3, and SN_4 are the inside diameter of the left and right holes, the outside diameter of the locating point, the height of the locating point, and the middle recess thickness, respectively. The results are shown in *Table 5*. The SN ratio of various quality characteristics is standardized by *Eq. (5)*, and the matrix $[S_{ij}]$ is obtained, i.e., the standardized value of the SN ratio of the No. j quality characteristic in the No. i parameter combination, as shown in *Table 6*.

$$\left[S_{ij}\right]=\frac{\left[x_{ij}\right]-\min\left[x_{ij}\right]}{\max\left[x_{ij}\right]-\min\left[x_{ij}\right]} \quad , \quad (i=1,2,\ldots,l;\ j=1,2,\ldots,m) \tag{5}$$

Table 5. Original SN ratio matrix.

No.	SN_1	SN_2	SN_3	SN_4
1	44.37	33.14	32.21	22.42
2	35.05	36.78	23.43	34.72
3	44.45	47.28	31.14	31.31
4	31.33	41.29	27.09	29.66
5	27.6	23.61	34.26	38.43
6	33.47	24.95	24.1	24.29
7	33.81	41.02	40.8	17.15
8	32.86	30.11	25.4	25.83

Table 6. Standardized SN ratio matrix.

RUN	S_{J1}	S_{J2}	S_{J3}	S_{J4}
1	0.996	0.403	0.505	0.248
2	0.442	0.557	0	0.826
3	1	1	0.444	0.666
4	0.221	0.747	0.211	0.588
5	0	0	0.623	1
6	0.349	0.057	0.038	0.336
7	0.369	0.735	1	0
8	0.312	0.275	0.113	0.408

Step 2: the matrix of the correlation coefficient, eigenvalue, coefficient of determination and eigenvector are calculated.

The correlation coefficient of the standardized SN ratio is calculated by *Eq. (6)*, and the correlation matrix [R] is obtained, as shown in *Table 7*. The matrix of the correlation coefficient, eigenvalue and eigenvector relation are expressed as *Eq. (7)*, and the matrix of the correlation coefficient, eigenvalue and eigenvector can be obtained. The coefficient of determination of various principal components is obtained by *Eq. (8)*, and the results are shown in *Table 8* and *Table 9*.

$$[\gamma_{jj'}] = \frac{\sum_{i=1}^{l}(S_{ij} - \overline{S_j})(S_{ij'} - \overline{S_{j'}})}{\sqrt{\sum_{i=1}^{l}(S_{ij} - \overline{S_j})^2 \sum_{i=1}^{l}(S_{ij'} - \overline{S_{j'}})^2}}. \quad (6)$$

Where $\gamma_{jj'}$ is the coefficient of the correlation between the No. j quality characteristic and the No. j' quality characteristic, $\overline{S_j}$ is the average of the standardized SN ratios of the experimental groups of the No. j quality characteristic, and $\overline{S_{j'}}$ is the average of the standardized SN ratios of the experimental groups of the No. j' quality characteristic.

$$\left|\left[\gamma_{jj'}\right] - \lambda_p I_{m\times m}\right|\beta_p = 0, (p = 1,2,3,4). \quad (7)$$

$$C_p = \frac{\lambda_p}{T}. \quad (8)$$

Where λ_p is the eigenvalue of the No. p principal component, $I_{m\times m}$ is the m×m unit matrix, β_p is the eigenvector corresponding to λ_p of the No. p principal component, C_p is the coefficient of determination of the No. p principal component, and T is the total eigenvalue of various principal components.

Table 7. Matrix of correlation coefficients.

	γ_{j1}	γ_{j2}	γ_{j3}	γ_{j4}
$\gamma_{1j'}$	1	0.5107	0.0675	-0.2771
$\gamma_{2j'}$	0.5107	1	0.2239	-0.1554
$\gamma_{3j'}$	0.0675	0.2239	1	-0.3415
$\gamma_{4j'}$	-0.2771	-0.1554	-0.3415	1

Table 8. Eigenvalue and coefficient of determination.

Component	Eigenvalue	Coefficient of determination
Principal component 1	1.801	45.01%
Principal component 2	1.061	26.52%
Principal component 3	0.729	18.22%
Principal component 4	0.41	10.25%

Table 9. Eigenvectors of principal components.

Quality characteristic	Eigenvector Principal component 1	Principal component 2	Principal component 3	Principal component 4
The inside diameter of the left and right holes	0.5524	0.4689	-0.2666	0.6356
Outside diameter of locating point	0.5567	0.3921	0.43	-0.5928
Height of locating point	0.4034	-0.6413	0.549	0.3529
Middle recess thickness	0.4714	0.4638	0.6653	0.3466

Step 3: Calculate the principal component score and multiple performance characteristic index (MPCI)

The principal component scores and MPCI Ω_i are calculated by *Eq. (9)* and *Eq. (10)*, respectively, where Φ_{ip} is the score of the No. p principal component in the No. i experimental group, and β_{ip} is the eigenvector corresponding to the No. p principal component. The results are shown in *Table 10*.

$$\Phi_{ip} = \sum_{j=1}^{4} \beta_{ip} S_{ij}. \quad \textbf{(9)}$$

$$\Omega_i = C_p \times \Phi_{ip}. \quad \textbf{(10)}$$

Table 10. Principal component score and MPCI.

Experimental group	Principal component score				MPCI
	Principal component 1	Principal component 2	Principal component 3	Principal component 4	
Standard column	1.984	0.684	1.378	0.742	
1	1.095	0.416	0.35	0.658	0.734
2	0.943	0.809	0.671	0.237	0.786
3	1.602	0.885	0.85	0.43	1.155
4	0.9	0.534	0.769	-0.024	0.684
5	0.723	0.064	1.007	0.567	0.584
6	0.398	0.317	0.176	0.318	0.328
7	1.016	-0.18	0.767	0.151	0.565
8	0.563	0.371	0.368	0.217	0.441

Step 4: determine the factor level combination of the optimum parameters

The total score response table of various parameters at different levels is calculated. The results indicated the material should be PLA, a fill thickness of 0.16mm, a wall thickness of 0.8mm, a bottom/top thickness of 1.2mm, an infill density of 50%, a printing speed of 20mm/s, and an extruder head temperature of 220℃. The optimum printing parameter combination was A1 B2 C2 D1 E1 F2 G2, as shown in *Table 11*.

Table 11. Principal component total score response table.

Control factor	Material	Fill thickness	Wall thickness	Bottom/top thickness	Infill density	Printing speed	Extruder head temperature
Level 1	0.84	0.608	0.632	0.759	0.664	0.611	0.578
Level 2	0.479	0.711	0.688	0.56	0.655	0.708	0.741
Optimum level	A1	B2	C2	D1	E1	F2	G2

5|Confirmation Experiment

The confirmation test was implemented for the aforesaid optimum printing parameter combination. Four clip body samples were printed to judge whether they could fall in the CI and meet the specification tolerance.

5.1|In Confidence Interval

First, the SN ratio under the optimum printing parameter combination was predicted using *Eq. (11)*, in which SN is the overall average SN of all experimental groups and $\overline{A_1}, \overline{B_2}, \overline{C_2}, \overline{D_1}, \overline{E_1}, \overline{F_2}, \overline{G_2}$ are the average SN ratio of various control factors under the optimum level condition, respectively. The 95% CI of the predicted SN ratio of various response values was calculated using *Eq. (12)*. The results are shown in *Table 12*. The measurement results of different quality characteristics fell into the CI, meaning the additive model of relevancy of various control factors was tenable, and there was no significant interaction among parameters.

$$SN = \overline{T} + (\overline{A_1} - \overline{T}) + (\overline{B_2} - \overline{T}) + (\overline{C_2} - \overline{T}) + (\overline{D_1} - \overline{T}) + (\overline{E_1} - \overline{T}) + (\overline{F_2} - \overline{T}) + (\overline{G_2} - \overline{T}).$$

$$CI = \sqrt{F_{\alpha;1;V_2} \times V_e \times \left[\frac{1}{n_{eff}} + \frac{1}{r}\right]}. \quad (11)$$

$$n_{eff} = \frac{L}{1 + Df^*}. \quad (12)$$

Where α is the significance level (α=0.05), v is the DOF of the pooled error variance, Ve is the pooled error variance, neff is the number of effective observations, L is the total instances of processing (L=8), Df* is used to estimate the total DOF of factors of the mean value, and r is the sample number for the confirmation test (r=4).

Table 12. Confirmation test sample quality characteristics in CI.

Quality characteristic	Predicted value	95% CI	True mean
The inside diameter of the left and right holes	46.894	43.024~50.764	44.519
Outside diameter of locating point	49.903	44.832~54.973	47.424
Height of locating point	40.076	34.401~45.751	36.686
Middle recess thickness	39.52	29.724~49.316	33.559

5.2|Meeting the Specification Tolerance

The size feature of the clip body 3D model built by the drawing software was the target value, and whether the size feature of the four quality characteristics of the printed samples in the confirmation test was within the specification tolerance was judged. The results are shown in *Table 13*. The four quality characteristics of the printed samples were within the specification tolerance.

Table 13. Confirmation test of the sample quality characteristics.

Quality characteristic	Target value	Tolerance range	Confirmation test sample size feature			
The inside diameter of the left and right holes	2.385	2.350~2.420	2.365	2.359	2.39	2.38
Outside diameter of locating point	1.606	1.543~1.669	1.613	1.613	1.602	1.6
Height of locating point	0.901	0.783~1.019	0.925	0.925	0.953	0.942
Middle recess thickness	1.185	1.049~1.321	1.24	1.2	1.22	1.26

5.3 | Benefit Assessment

This study used a 3D printing technique to produce components for the electronics manufacturing industry to evaluate the benefits. The cost of production was estimated, including the equipment cost, labour cost, and material cost. The equipment cost consisted of the purchase cost of the 3D printing machine and the depreciation and amortization cost during production. The labour cost included creating the 3D model file, operating the printing machine object, the subsequent surface treatment, and component assembly. The material cost covered the materials for the print object and the support structure. The benefit of using 3D printing to produce components for the electronics manufacturing industry is expressed as Eq. 13, in which V_p is the component value (price), T_p is the total production hours, t_p is the time needed to print the component, C_{3D} is the acquisition cost of the 3D printing machine, r_d is the depreciation rate per unit time of the 3D printing machine, $\sum(t_p \times r_o)$ is the sum of the products of the component printing, subsequent surface treatment and assembly time and the corresponding unit salary of the operators, C_m is the material cost for printing the component, t_m is the time needed for component size measurement and modelling, and r_e is the salary per unit time of the modelling engineer.

$$\texttt{Benefit}=\left(V_p \times \frac{T_p}{t_p}\right) - \left\{\left[\left(C_{3D} \times r_d \times t_p\right) + \sum(t_p \times r_o) + C_m\right] \times \frac{T_p}{t_p} + (t_m \times r_e)\right\}. \quad \textbf{(13)}$$

6 | Conclusion

This study aimed to introduce 3D printing techniques into the electronics manufacturing industry, taking the printing of an AI parts clip body as an example. First, the loss from machine stoppage or maintenance resulting from failed assembly or machine interference when the component quality failed to meet the standard was considered, the rework cost resulting from the component failing to meet specifications was evaluated, and the range of allowable errors for normal operation of the printed component on the machine was determined. The tolerance determination of the Taguchi quality loss method established the printed clip body manufacturer tolerance.

Secondly, a printing parameter optimization experiment was conducted to upgrade the overall quality. The key quality characteristics of the clip body were considered, including the inside diameter of the left and right holes, the outside diameter of the locating point, the height of the locating point, and the middle recess thickness. The control factors were the material, fill thickness, and printing speed. PCA was combined with the four quality above characteristics to propose the optimum parameter combination: PLA material, a fill thickness of 0.16mm, a wall thickness of 0.8mm, a bottom/top thickness of 1.2mm, an infill density of 50%, a printing speed of 20mm/s, and an extruder head temperature of 220℃.

Finally, the benefits of using 3D printing techniques to produce components for the electronics manufacturing industry were assessed. The production costs included the 3D printing machine purchase cost, depreciation, and amortized cost, the labour cost of creating the 3D model file, the cost of operating the

printing machine object, the subsequent surface treatment and component assembly, and the material cost of the print object and support structure.

Author Contribution

C.-Y. Huang: Methodology, Software, Validation, Formal analysis, and investigation. Y.-W. Chung: Writing, creating the initial design, conceptualization, and editing.

All authors have read and agreed to the published version of the manuscript.

Funding

This research received no external funding.

Data Availability

All the data are available in this paper.

Conflicts of Interest

The authors declare no conflict of interest.

References

[1] Bogue, R. (2013). 3D printing: the dawn of a new era in manufacturing? *Assembly automation*, *33*(4), 307–311. https://doi.org/10.1108/AA-06-2013-055

[2] Chen, J. C., & Gabriel, V. S. (2016). Revolution of 3d printing technology and application of six sigma methodologies to optimize the output quality characteristics. *International conference on industrial technology (ICIT)* (pp. 904–909). Taipei, Taiwan. IEEE. https://doi.org/10.1109/ICIT.2016.7474872

[3] Sanatgar, R. H., Campagne, C., & Nierstrasz, V. (2017). Investigation of the adhesion properties of direct 3D printing of polymers and nanocomposites on textiles: effect of FDM printing process parameters. *Applied surface science*, *403*, 551–563. https://doi.org/10.1016/j.apsusc.2017.01.112

[4] Zhang, Y., Qian, Z. S., Sprei, F., & Li, B. (2016). The impact of car specifications, prices and incentives for battery electric vehicles in Norway: choices of heterogeneous consumers. *Transportation research part c: emerging technologies*, *69*, 386–401. https://doi.org/10.1016/j.trc.2016.06.014

[5] Panda, B., Shankhwar, K., Garg, A., & Savalani, M. M. (2019). Evaluation of genetic programming-based models for simulating bead dimensions in wire and arc additive manufacturing. *Journal of intelligent manufacturing*, *30*, 809–820. https://doi.org/10.1007/s10845-016-1282-2

[6] Zhang, Y., Bernard, A., Harik, R., & Karunakaran, K. P. (2017). Build orientation optimization for multi-part production in additive manufacturing. *Journal of intelligent manufacturing*, *28*, 1393–1407. https://doi.org/10.1007/s10845-015-1057-1

[7] Huang, C.-Y., & Lin, Y.-H. (2013). Applying CHAID algorithm to investigate critical attributes of void formation in QFN assembly. *Soldering & surface mount technology*, *25*(2), 117–127. https://doi.org/10.1108/09540911311309086

[8] Yang, K., Gan, Y., Cao, Y., Yang, J., & Wu, Z. (2023). Optimization of 3D tolerance design based on cost-quality-sensitivity analysis to the deviation domain. *Automation*, *4*(2), 123–150. https://doi.org/10.3390/automation4020009

[9] Naresh, B., & Reddy, A. C. (2023). An intelligent framework based on the integration of GRA, fuzzy logic, and Taguchi's approaches for multi-response optimization of wire-EDT process parameters. *International journal on interactive design and manufacturing (IJIDEM)*, *17*(6), 3211–3228. https://doi.org/10.1007/s12008-023-01381-x

[10] Huang, C.-Y., Huang, H.-H., & Ying, K.-C. (2012). Sn-Cu-Ni soldering process optimization using multivariate analysis. *IEEE transactions on components, packaging and manufacturing technology*, *2*(3), 527–535. https://doi.org/10.1109/TCPMT.2011.2177093

[11] Huang, C. Y. (2012). Intelligent parametric design for a robust LED encapsulation process. *IEEE transactions on components, packaging and manufacturing technology*, *2*(11), 1919–1927. https://doi.org/10.1109/TCPMT.2012.2210221

[12] Fernández-Rubiera, J. Á., Barbón, A., Bayón, L., & Ghodbane, M. (2023). Sawtooth V-trough cavity for low-concentration photovoltaic systems based on small-scale linear fresnel reflectors: optimal design, verification, and construction. *Electronics*, *12*(13), 2770. https://doi.org/10.3390/electronics12132770

[13] Huang, C. Y., Chen, C. H., & Lin, Y. H. (2016). A grey-ANN approach for optimizing the QFN component assembly process for smart phone application. *Soldering & surface mount technology*, *28*(2), 63–73. https://doi.org/10.1108/SSMT-10-2015-0034

[14] Georgantzinos, S. K., Kastanos, G., Tseni, A. D., & Kostopoulos, V. (2023). Efficient optimization of the multi-response problem in the Taguchi method through advanced DEA formulations integration. *Available at ssrn 4494080*. https://dx.doi.org/10.2139/ssrn.4494080

[15] Huang, C. Y., & Tsai, P. X. (2024). Applying machine learning to construct a printed circuit board gold finger defect detection system. *Electronics*, *13*(6), 1090. https://doi.org/10.3390/electronics13061090

[16] Chandgude, S., Pawar, P., & Sadaiah, M. (2015). Process parameter optimization based on principal components analysis during machining of hardened steel. *International journal of industrial engineering computations*, *6*(3), 379–390. http://dx.doi.org/10.5267/j.ijiec.2015.2.004

[17] Bharadiya, J. P. (2023). A tutorial on principal component analysis for dimensionality reduction in machine learning. *International journal of innovative science and research technology*, *8*(5), 2028–2032. https://www.researchgate.net/profile/Jasmin-Bharadiya

[18] Bruin, B. J. (2020). PCA and EFA with SPSS. UCLA: statistical methods and data analytics. Retrieved March 21, 2022. https://stats.oarc.ucla.edu/spss/seminars/efa-spss

[19] Mian Qaisar, S., & Hussain, S. F. (2023). An effective arrhythmia classification via ECG signal subsampling and mutual information based subbands statistical features selection. *Journal of ambient intelligence and humanized computing*, *14*(3), 1473–1487. https://doi.org/10.1007/s12652-021-03275-w